Author(s): Klingler, Sarah; Bagemihl, Benedikt; Mengele, Aexander; Kaufhold, Simon; Myllyperkiö, Pasi; Ahokas, Jussi; Pettersson, Mika; Rau, Sven; Mizaikoff, Boris

Title: Rationalizing In Situ Active Repair in Hydrogen Evolution Photocatalysis via Non-Invasive Raman Spectroscopy

Year: 2023

Version: Published version

How to cite: *Angew. Chem. Int. Ed.* **2023**, *62*, e202306287
doi.org/10.1002/anie.202306287

Photocatalysis

Rationalizing *In Situ* Active Repair in Hydrogen Evolution Photocatalysis via Non-Invasive Raman Spectroscopy

Sarah Klingler[+], Benedikt Bagemihl[+], Alexander K. Mengele, Simon Kaufhold, Pasi Myllyperkiö, Jussi Ahokas, Mika Pettersson, Sven Rau, and Boris Mizaikoff**

Abstract: Currently, most photosensitizers and catalysts used in the field of artificial photosynthesis are still based on rare earth metals and should thus be utilized as efficiently and economically as possible. While repair of an inactivated catalyst is a potential mitigation strategy, this remains a challenge. State-of-the-art methods are crucial for characterizing reaction products during photocatalysis and repair, and are currently based on invasive analysis techniques limiting real-time access to the involved mechanisms. Herein, we use an innovative *in situ* technique for detecting both initially evolved hydrogen and after active repair via advanced non-invasive rotational Raman spectroscopy. This facilitates unprecedently accurate monitoring of gaseous reaction products and insight into the mechanism of active repair during light-driven catalysis enabling the identification of relevant mechanistic details along with innovative repair strategies.

[*] S. Klingler,[+] Prof. Dr. B. Mizaikoff
Institute of Analytical and Bioanalytical Chemistry, Ulm University
Albert-Einstein-Allee 11, 89081 Ulm (Germany)
E-mail: boris.mizaikoff@uni-ulm.de

B. Bagemihl,[+] Dr. A. K. Mengele, Dr. S. Kaufhold, Prof. Dr. S. Rau
Institute of Inorganic Chemistry I, Ulm University
Albert-Einstein-Allee 11, 89081 Ulm (Germany)
E-mail: sven.rau@uni-ulm.de

Dr. P. Myllyperkiö, Dr. J. Ahokas, Prof. Dr. M. Pettersson
Department of Chemistry, Nanoscience Center, University of Jyväskylä
40014 University of Jyväskylä (Finland)

Dr. J. Ahokas
Financial and Facility Services, University of Jyväskylä
40014 University of Jyväskylä (Finland)

Prof. Dr. B. Mizaikoff
Hahn-Schickard
Sedanstraße 4, 89081 Ulm (Germany)

[+] These authors contributed equally to this work.

Introduction

The steadily increasing global energy consumption drives the need for replacing fossil energy resources with renewable alternatives.[1] Since fossil energy resources such as coal, petroleum and natural gas are finite and the cumulative production of pollutant flue gases including but not limited to CO_2, NO_x and SO_x leads to global warming and health issues. Hence, the transition to safe, clean and sustainable energy resources is among the most prevalent scientific and technological global challenge of the 21st century.[1–3]

Light-driven water splitting converts solar energy into usable chemical energy generating non-polluting oxygen and hydrogen gas, which represents a carbon-free fuel with the highest energy content relative to molecular weight.[4,5] Hydrogen can be stored and converted into electricity on demand via fuel cell technology with high energy conversion efficiencies and without producing greenhouse gas emissions. Consequently, light-driven water splitting provides an attractive solution for storing energy provided by sunlight, that recently even could be achieved using low-energy NIR-light.[6] Hence, natural photosynthesis remains the inspiration for the development of efficient artificial light-to-chemical energy conversion strategies.[7–11]

Deterioration and degradation processes are an inherent limitation of catalytic systems[12] triggering research into methods to repair catalytic centers and revitalize catalytic activity,[13–15] as recently reviewed.[16]

Pfeffer et al. have discovered an active repair strategy for their dinuclear photocatalyst ($[(tbbpy)_2Ru(tpphz)PtI_2](PF_6)_2$ (**RuPtI$_2$**, with tbbpy = 4,4′-di-*tert.*-butyl-2,2′-bipyridine, tpphz = tetrapyrido[3,2-a:2′,3′-c:2″,3″-h:2‴,3‴-j]phenazine and PF_6^- = hexafluorophosphate anion)).[17] This photocatalyst can be revived by a strong oxidant after hydrogen evolution catalysis with triethylamine, mimicking nature's inherent ability to deal with inactive catalytic centers in natural photosynthesis.[18] This led to an overall improvement of catalytic activity to accumulated turnover numbers >3000. However, the proposed repair step, based on $^1O_2$, is not orthogonal to the catalytic reaction, and therefore required removal of the catalysis medium. Furthermore, no detailed kinetic analysis of the pre- and post-repair activity was possible due to evolved hydrogen analysis via conventional gas chromatography (GC). During catalytic system optimization, mechanistic analysis or reaction monitoring, continuous *in situ* analysis methods are preferred not only facilitating real-time monitoring of the reaction products, but also for evaluating performance and efficiency.

In turn, detailed kinetic insight into product formation efficiencies would facilitate deliberate tuning of photocatalytic systems and reaction conditions and a comprehensive understanding of the catalyst lifecycle and mechanistic details.

To date, the "gold standard" for gas analysis remains to be head-space gas chromatography coupled to various detection schemes, and is the routine method for determining turnover numbers (TONs) and turnover frequencies (TOFs).[18,19] While GC offers high sensitivity and selectivity, it usually requires substantial instrumental investments and extended measurement times. Moreover, a sampling step is required using invasive access to the photocatalytic reaction compartment risking contamination, leakage and potentially significant consumption of analyte, which is of particular relevance in micro-reactors. Consequently, continuous reaction product monitoring would lead to a more comprehensive understanding of the entire photocatalytic scenario.

Commonly applied alternative analytical techniques include electrochemical sensors such as Clark-type electrodes,[20–25] microelectrochemical approaches,[26–28] and variants of mass spectrometry (MS).[9,29–31] While some of these methods allow fast measurements (ms/μs regime), and/or provide the desired reproducibility and low detection limits, they again either require invasive access to the reaction compartment or the discontinuous collection of samples at appropriate time intervals.[21]

Optical analysis methods offer an interesting alternative, as they potentially enable rapid and non-invasive diagnostics even in small sample volumes. Such optical sensors based on luminescence quenching are already in use for non-invasive oxygen monitoring.[32–37] Schiel et al.[38] introduced rotational Raman spectroscopy as a possible strategy for monitoring and evaluating a variety of gases. Recently, Schwarz et al.[39] described a device applied for the detection of H_2 and O_2 gas in a prototypic photocatalytic process employing rotational Raman spectroscopy confirmed as an *in situ* identification and quantification method for application times up to 8 h. Next to the inherent molecular selectivity, this technology facilitates non-invasive direct analysis, as especially demanded in photocatalytic micro-environments.

Herein, we discuss details of a new methodology for active repair in **$RuPtI_2$** addressing the limitations based on the established $^1O_2$ method using rotational Raman spectroscopy (i.e., NINGAS Analyzer (NGA)[39]) via a unique sampling interface facilitating the evaluation of rotational Stokes Raman lines characteristic for H_2. Specifically, this approach provides unique insight into the kinetics of the catalytic conversion pre- and post-repair analyzing the hydrogen evolution at **$RuPtI_2$**, leading to a more practicable methodology for economical usage of rare earth metal photocatalysts and thus demonstrating a generic characterization strategy.

Results and Discussion

Properties of the NGA

The NINGAS Analyzer was developed and designed to specifically meet requirements for the detection of gases relevant in artificial photosynthesis including H_2, O_2, N_2, CO_2 and CO via the evaluation of rotational Stokes Raman bands.[39,40] Exemplary spectra of these gases are shown in Figure S1 to underline the versatility of the device. A detailed description of the system is provided elsewhere,[39] only critical system improvements are reported herein. Raman measurements are performed in a back-scattering geometry particularly facilitating the detection of the rotational Raman spectrum of gaseous samples in enclosed reaction compartments (see Supporting Information, A.3).[39] The detection range of 40 to 645 cm^{-1} was determined empirically by analyzing standard solutions and solids (i.e., herein: CaF_2 (s), toluene (l), acetonitrile (l), cyclohexane (l), polystyrene (s), and carbon tetrachloride (l)) providing unobstructed spectral features in the expected wavenumber region by correlating the pixel position of the Raman bands with the wavenumber position according to literature (see Supporting Information, B.1). As temperature control is critical for ensuring the long-term system stability necessary for extended photocatalytic experiments, active heat dissipation at the excitation laser during operation is essential over periods of days (see Figure S5 and detailed discussion in Supporting Information, B.4).

Illumination and reaction heat may lead to evaporation and condensation of solvent droplets at the glass walls of the reaction compartment causing radiation scattering and attenuation. For facilitating the analysis of vaporizing reaction solutions and to prevent droplet formation, a reaction compartment with integrated heating system for temperature stabilization was developed (Figure 1). Likewise, any fogging or condensation effects at the glass compartment were effectively avoided when adjusting the temperature to a given solvent mixture. The vial holder comprises two segments (C and D) for glass vials with a volume of approx. 4 mL (E). Innovatively, the vials are mounted upside down such that the catalytic solution effectively acts as an additional seal, thereby excluding any leakage of hydrogen from the reaction compartment. The top part (D) was made from aluminum ensuring appropriate heat conduction, while the bottom part (C) was 3D-printed from black PLA serving as insulation avoiding additional heating of the sample solution, which could affect photo-induced reactions. All system components were blackened to avoid any scattering effects. With a heating cartridge (A) and temperature sensor (B) the temperature was accurately controlled and maintained constant. The sample holder is readily adjustable for larger reaction compartments and alternative illumination sources. This assembly ensures that the reported concentration values of the reaction product within this "inverted head-space" are unprecedently close to the true values when calculating TON or TOF numbers, as any leakage via a septum or any type of sealing of the vial is effectively avoided. It should be noted that conventional

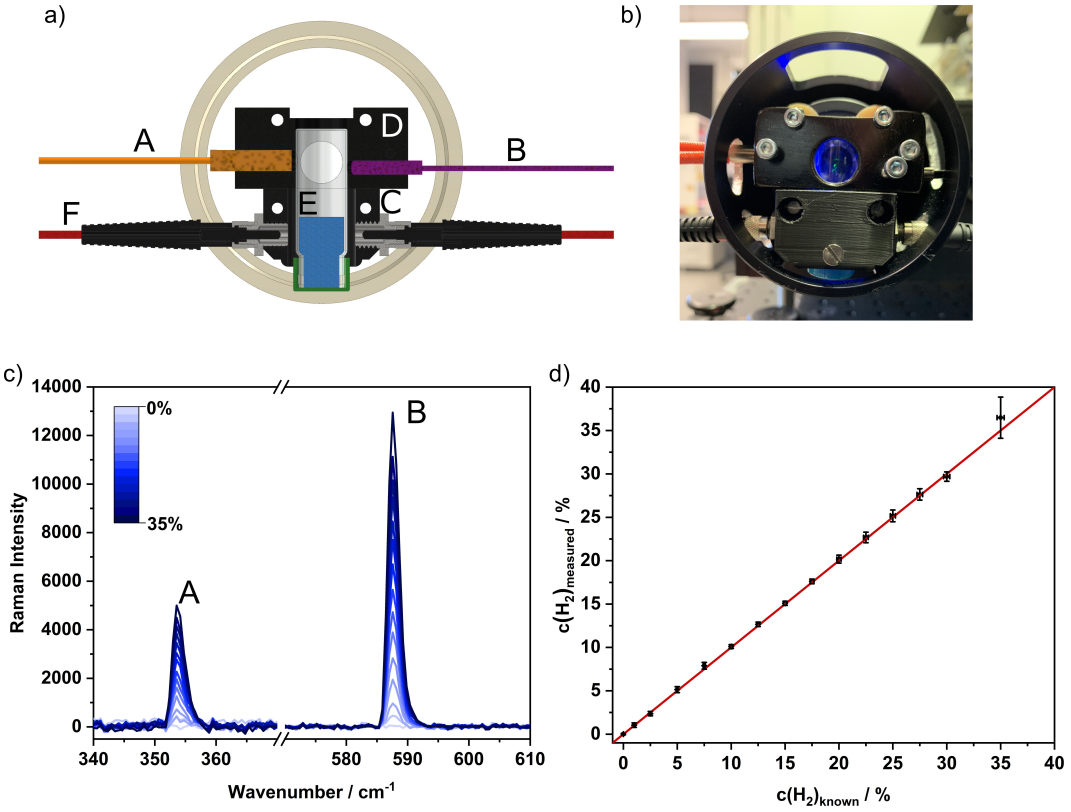

Figure 1. Advanced rotational Raman analyzer for long-term photocatalytic studies. (a) Schematic half-sectional view and (b) image of the developed sampling interface uniquely facilitating precise monitoring of gaseous reaction products during light-driven catalysis avoiding condensation of solvent droplets via integrated heating system for temperature stabilization. A: heating cartridge; B: temperature sensor; C: bottom part of sample holder (3D-printed from PLA); D: top part of the sample holder (blackened aluminum for efficient heat conduction), E: upside down sample compartment (glass vial) excluding leakage, F: fiber-coupled LED ($\lambda = 470$ nm, 97.0 ± 1.6 mW with 1000 µm fiber and 135.5 ± 5.0 mW with 1500 µm fiber). (c) Rotational Raman spectra (background corrected) for H_2 in argon (0–35 %) (v%). Peak A: rotational Raman band of para-H_2; Peak B: rotational Raman band of ortho-H_2.[54] (d) Comparison of merged measurement data sets compared to the ideal $c(H_2)_{measured}/c(H_2)_{known} = 1$ (red line) (collected on day 1 and 3; $n = 3$ for each day). Errors along the *x*-axis reflect the maximum error calculated based on the accuracies of the mass flow controllers of the gas mixing system; error along the *y*-axis reflects the standard deviation of the 6 measurements across three days.

glass vials are sufficient for these Raman studies, i.e., no specific cuvettes are required.

To demonstrate the accuracy and long-term stability required for extended *in situ* measurement periods frequently required in photocatalytic hydrogen production, a continuous study was performed over a period of three days.

For this purpose, 15 gas mixtures of H_2 in argon at defined H_2 concentrations in the range of 0–35 % (v%) (0 %, 1 %, 2.5 %, 5 %, 7.5 %, 10 %, 12.5 %, 15 %, 17.5 %, 20 %, 22.5 %, 25 %, 27.5 %, 30 %, and 35 %) were analyzed in a flow-through configuration. In Figure 1-c, the rotational Raman spectra of these control samples are exemplarily shown. Both, the ortho- and para-H_2 band were used for the quantitative evaluation based on previously recorded calibration spectra (see Supporting Information, A.7).[39]

Figure 1-d shows the reliability of the measurements during long-term studies. The comparison includes merged data sets of measurements collected on day 1 and 3 compared to the ideal accuracy of $c(H_2)_{measured}/c(H_2)_{known} = 1$ indicated by the red line with the NGA Analyzer measuring continuously. While the standard deviation (i.e., *y*-error) increases with increasing concentration of hydrogen, the determined concentrations fit the real concentrations exceptionally well, thus corroborating the demanded accuracy over large concentration ranges of H_2. The obtained results also indicate sufficient long-term stability as demanded during photocatalytic experiments with variations only in the minute-range caused mainly by the fluctuations of the laser power during continuous operation. For a more detailed evaluation of the laser stability, an extended laser stability test was performed (see Supporting Information, Chapter A.11).

Rotational Raman studies on photocatalytic hydrogen production

To follow an actual photocatalytic process, the **$RuPtI_2$** ($[(tbbpy)_2Ru(tpphz)PtI_2](PF_6)_2$) system was exemplarily investigated. This system shows a turnover performance ideally suited to be tested by the optimized Raman system vs. the data shown by Pfeffer et al.[17,18] Therefore, 2 mL of a

50 μM catalyst solution in a 6:3:1 mixture of acetonitrile, triethyl amine and water (ACN:TEA:H_2O respectively, v:v:v) in a glass vial was illuminated from the side via one or two fiber-coupled LEDs emitting at 470 nm (F-LED, Figure 1-a and b). The wavelength was determined most suitable based on previous reports for Ru-tpphz-based photocatalysts.[17,41] During illumination the amount of hydrogen generated by the photocatalytic reaction was analyzed continuously (see also Supporting Information, A.10). The sample volume of catalytic solution required for the Raman measurement equals only $^1/_4$ of the amount necessary for a GC measurement, i.e. 2 mL instead of 8 mL used by Pfeffer et al..[17] It should be noted that the amount of catalytic solution could even be further reduced, depending on the amount of evolved hydrogen.

Figure 2 shows the comparison of the determined TONs between the GC measurement and two repetitions of the Raman measurements under illumination with one F-LED (for a detailed description on TON calculations see Supporting Information, A.4). In this comparison, for the GC measurements a volume of 8 mL of 50 μM photocatalyst in catalytic solution (in ACN:TEA:H_2O respectively, v:v:v) was transferred to a Schlenk flask inside an argon-filled glovebox (see Supporting Information, Chapter A.12).

This sample was then irradiated using four LED strips with light power comparable to the F-LED used during the Raman studies. After optimization, the exposure time (i.e., illumination time of the sample exposed to the laser light)[42] of the sample in the Raman system was set to 25 s and each measurement was collected in time intervals of 600 s. Thus, significantly more data points are generated in the same observation period vs. conventional GC measurements, which is limited to invasive sampling and possible contamination as well as potential perforation of the reaction compartment when sampling from the same compartment through a septum. If needed, a higher data rate at even shorter time intervals is possible, as the minimal time gate between individual measurements is primarily limited by the required exposure time of the sample (i.e., in general, lower concentrations require extended exposure times). Given the significantly more detailed trajectory provided by the Raman data compared to previous GC measurements, for the first time an induction phase of the hydrogen evolution catalysis is clearly identified for **$RuPtI_2$** (see Figure 2; first 30 h), as recently shown for $K_2[PtCl_4]$ using a $[Ru(bpy)_3]^{2+}$ photosensitizer.[43] For Ru^{II}-Pd^{II} dinuclear photocatalysts, induction phases are known to occur. Hammarström and coworkers hypothesized that Pd^0 colloid formation that was observed in a specific complex may be the reason for the observed induction period.[44] However, for Ru^{II}-tpphz-Pt^{II} photocatalysts this is not the case, as no Pt colloid formation could be determined.[45]

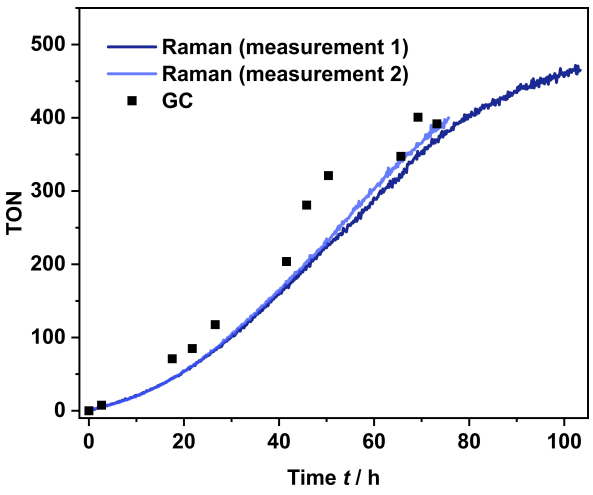

Figure 2. Comparison of GC vs. Rotational Raman data. Comparison of turn-over numbers (TONs) vs. time between Raman and exemplary GC data as well as comparison between two repetitive Raman measurements. Illumination was performed with one LED (λ = 470 nm, 97.0 ± 1.6 mW).

Additionally, the non-invasive *in situ* measurement capability highlights previous difficulties when determining the endpoint of a catalytic run using GC data (cf. GC data in Figure 2). While discontinuously collected data may suggest an alleged endpoint of catalysis after approx. 60 h, this was disproved via Raman data, which clearly indicated significantly longer active catalysis (cf. Raman data in Figure 2). Accurately characterizing low hydrogen evolution activity - as found during the induction period and during the final levelling off phase in hydrogen evolution catalysis - is of pivotal interest for improving next-generation catalytic systems, i.e., for fundamentally understanding the formation of the catalytically active species or for determining the final fate of a photocatalyst.

The intensity of irradiation determined at the rear end of the fiber (see SI, Chapter A.9 for a more detailed description) affected the amount of hydrogen produced (Figure 4-b), as observed for **$RuPtI_2$** by Pfeffer et al..[17] In contrast, almost no difference in the photocatalytic data between 194.0 ± 3.2 mW and 270.9 ± 9.9 mW is observed indicating that the number of photons is no longer limiting for the catalysis. In summary, given the minimal signal fluctuations observable within the Raman data trajectories it has been confirmed that continuous illumination during the entire experiment does not interfere with the Raman measurement. This underlines the suitability of this method for observing photocatalytic reactions across extended periods of time. In addition, when comparing the Raman measurements shown in Figure 2 excellent reproducibility - and comparability - is evident, which may not be achieved by discontinuous GC experiments requiring manual sample handling. The improved information depth of Raman studies vs. commonly practiced GC analysis is particularly evident when studying phases of the catalytic cycle characterized by low hydrogen production activity or at low irradiation intensities.

Rationalizing active repair via persulfate

Once the endpoint of the catalytic reaction has been reached, the sample solution shows a deep purple color. This indicates the full hydrogenation of the pyrazine ring

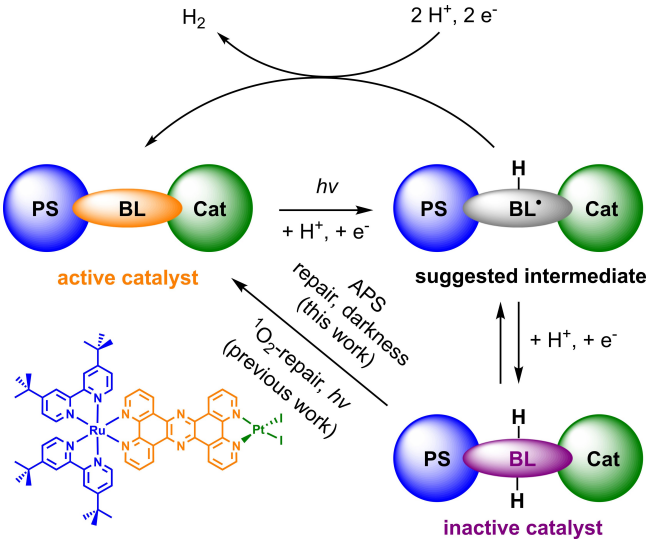

Figure 3. Catalysis and active repair for the hydrogen evolution catalysis of **$RuPtI_2$** (based on reference 18 and the kinetic data in Figure 5, S17 and S18). Abbreviations: 'hv' indicates irradiation with 470 nm (F−)LED in the 6:3:1 mixture (ACN:TEA:H_2O, v:v:v), PS = photosensitizing unit, BL = bridging ligand (tpphz), Cat = catalytic center. The color coding of the active catalyst is shown in the structure of **$RuPtI_2$** in the bottom left. The counterions of the complex are omitted for reasons of simplicity.

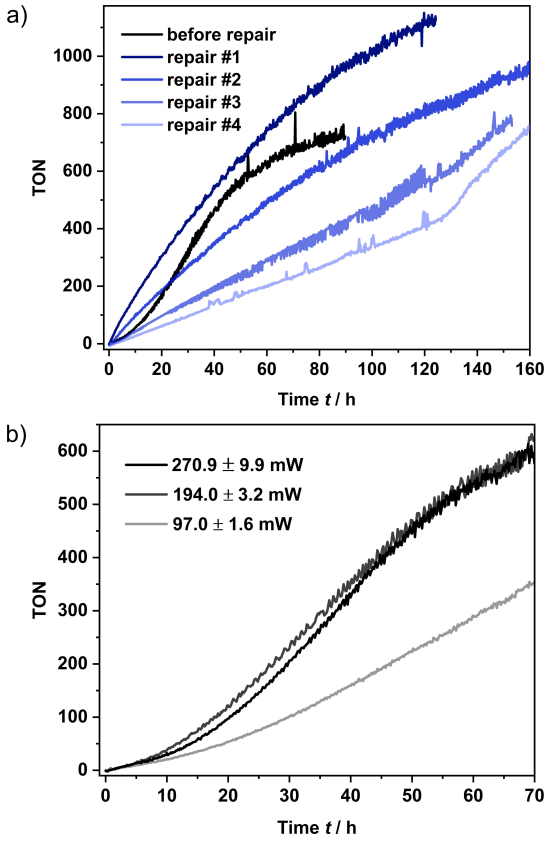

Figure 4. Comparison of the kinetics before and after active repair and at different irradiance. (a) Comparison of H_2 evolution before and after repair with 400 eq. APS while illuminating with two LEDs (470 nm, each 97.0 ± 1.6 mW; 69.84 µM catalyst solution, i.e. a total illumination power of 194.0 ± 1.6 mW). Note: For the 3rd repair measurement, the data between 14 h and 21 h are extrapolated due to an unexpected power outage of the computer discontinuing the data acquisition, for the 4th cycle, insoluble precipitate formation led to clouding of the solution. (b) Comparison of H_2 evolution when illuminating with different illumination intensities (70 µM catalyst solutions).

within the bridging tpphz ligand, which has previously been reported and discussed in detail, as it results in the deactivation of the light induced electron transfer to the catalytic center.[18] This effect is schematically shown in Figure 3 (assignment based on the UV/Vis spectroscopic data). Active repair of this inactive form of **$RuPtI_2$** has recently been shown via singlet oxygen acting as a strong oxidizing agent.[18] However, this procedure involves (i) removal of the catalysis medium (6:3:1 mixture of ACN:TEA:H_2O, v:v:v), (ii) re-dissolution, (iii) repair in pure and aerated ACN followed by (iv) irradiation at 470 nm, (v) removal of ACN, and finally, (vi) re-dissolution under argon in freshly degassed catalytic solvent mixture (6:3:1 mixture of ACN:TEA:H_2O, v:v:v). All of these steps introduce multiple potential sources of error and contamination. Therefore, in the present study after catalysis an *in situ* repair of the hydrogenated **$RuPtI_2$** catalyst was performed using $(NH_4)_2S_2O_8$ (ammonium persulfate, APS), an agent with proven oxidation activity, e.g., in wastewater treatment[46,47] and for chemical oxidations.[48] Hence, after removal of the catalytically developed hydrogen (i.e., by gas circulation in a glovebox with argon atmosphere) approx. 400 equivalents of APS with regard to **$RuPtI_2$** was added directly into the catalytic solution under an inert atmosphere. The catalyst was allowed to undergo repair undisturbed, i.e., APS was re-oxidizing the hydrogenated bridge in the dark for 30 min until the color of the solution changed back to red-orangish circumventing above-described steps (i-vi). Then the sample was sealed and subsequently exposed to another catalytic cycle, again analyzed via rotational Raman spectroscopy.

Figure 4-a shows the catalytic performance as TONs vs. time before and after repair of the photocatalyst with APS. In total, four repair steps were monitored, for which quantum yields between 0.03 and 0.06% could be estimated (see more details Chapter A.5 in the SI).

For studying the photocatalytic system before and after repair, the device was operated over a period of about 700 h (i.e., approx. 29 days). The catalytic studies were performed while illuminating with 2 F-LEDs; during repair periods only, the excitation laser of the Raman system was turned off, while the CCD camera remained cooled to −60 °C ensuring reproducible and comparable measurement conditions during the entire observation cycle.

It is clearly evident that the *in situ* Raman measurements provide yet unprecedented insight into the catalytic behavior of the photocatalyst before and after repair. Especially surprising was the absence of an induction period for the catalytic runs after repair in comparison to the run before repair (Figure 4-a). Consequently, the obtained data indicates significantly different kinetics for hydrogen evolution

after APS-based repair of the catalyst. Instead of revealing the newly identified induction phase observed for the pristine **$RuPtI_2$**, the hydrogen evolution curve rises immediately and follows a rather logarithmic behavior. For repair #3 and #4, the logarithmic behavior changes resembling an almost linear function. To rationalize this fundamentally different behavior before and after *in situ* repair via APS, the anticipated reaction product of active repair by APS, sulfate,[49] was added as soluble tetrabutylammonium hydrogen sulfate to a fresh catalytic sample. Thereby, the influence of APS product sulfate onto the catalysis can be studied. However, the resulting catalytic TON vs. time curve (see Figure S17) shows the same characteristic behavior compared to catalysis without APS or sulfate in Figure 4, which indicates that sulfate is not the origin of the disappearance of the induction phase. For fundamental understanding of the active repair step, the conditions during catalysis were replicated in a cuvette experiment as close as possible to the vial experiment, monitoring the changes via a fiber-optically coupled UV/Vis spectrometer at the timeframe of seconds. This timeframe is highly relevant to catalytic processes such as hydrogen formation and (de)activation of catalysts involving multiple fundamental steps including electron and proton transfer events.[50] To create conditions closely related to repair under catalytic conditions (see Figure 5), photochemically hydrogenated **$RuPtI_2$** was dissolved in a solution of ACN and TEA and a pre-dissolved solution of APS in water was added in one shot adding up to a total solvent composition of 6:3:1 (ACN:TEA:H_2O), i.e. catalytic solvent mixture conditions. Right after the addition UV/Vis spectra were recorded with a temporal resolution of one second for a period of 30 min, which is the period applied for the active repair cycle during catalytic measurements in the present study, against a background of the 6:3:1 solvent mixture.

The corresponding spectra (Figure 5-a at the example of 400 equivalents of APS) clearly indicate the decrease of the band at 570 nm, which has recently been attributed to the hydrogenated species.[18] With increasing concentrations of APS, the kinetics for oxidation of the hydrogenated species are accelerated (*cf.* Figure 5-b and Figure S10 for all associated spectra). Notably, the repair by APS does not proceed via a semi-hydrogenated species (see absence of a corresponding UV/Vis signal and of isosbestic points above 500 nm in Figure 3, top right), as this species would show an absorption band at 590 nm.[18] This suggests that fast two-electron-oxidation and connected release of two protons from the bridge occurs by APS and restores a catalytically active species.[51] For organic phenazine, this is known to occur on comparable timescales.[52,53] The resulting product from APS is therefore most likely sulfate. Remarkably, since this step is possible in darkness and in the mixture used for H_2 evolution catalysis, in contrast to the recently employed active repair by singlet oxygen,[18] this step can now be employed orthogonally to the catalysis within much shorter time. However, since 400 equivalents of APS are added at once, after active repair a large amount stays in the sample. To assess its effect on the catalysis, a sample of **$RuPtI_2$** was repaired in a cuvette in the catalytic mixture by 400 eq. APS

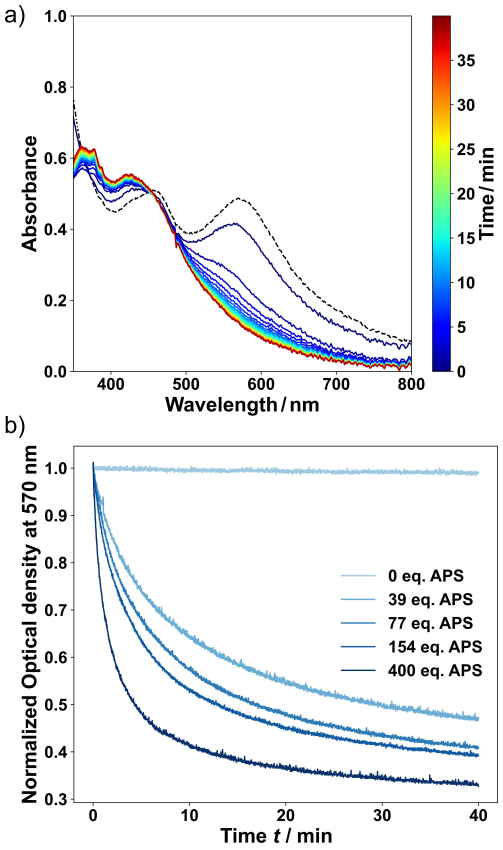

Figure 5. Active repair of $RuPtI_2$ using 400 equivalents of APS in the dark. A solution of **$RuPtI_2$** was stirred in ACN:TEA when APS in water was added and the cuvette was shaken. (a) Spectral traces obtained with a time span of 100 s between the spectra with 400 equivalents of APS present. The black dashed curve is the initial spectrum without APS and was recorded separately under equal conditions. (b) Temporal evolution of the signal at 570 nm for variable concentrations of APS with 1 s between datapoints.

and a subsequent catalysis was performed followed by UV/Vis spectroscopy, as depicted in Chapter B.8 in the SI. The results of this investigation show a significantly reduced absorbance at 570 nm, which indicates the reduced formation of the deactivated, hydrogenated **$RuPtI_2$**. This behavior might indicate a continuous repair of the photocatalyst by leftover APS during catalysis. This prevents accumulation of hydrogenated **$RuPtI_2$** and thus might be leading to changed catalysis kinetics compared to the pristine **$RuPtI_2$**.

Derived from the utilization in wastewater treatment, APS is known to form strongly oxidizing radical species,[47] that might have destructive power to the photocatalyst. However, this destruction for **$RuPtI_2$**, was only found when irradiated in the presence of APS in acetonitrile:water (8:2, v:v) without the sacrificial electron donor TEA present (see Figure S14 in SI). Without irradiation of the solution, a situation reminiscent to the active repair, no MLCT-decay of the complex was detected, thereby effectively avoiding the more destructive sulfate radical.[49] Therefore, in the darkness (i.e. at ambient light) any side reactions should be suppressed ensuring exclusive and direct oxidation of hydro-

genated **$RuPtI_2$** by APS, as schematically shown in Figure 3. The integrity of persulfate at the applied conditions (6:3:1 mixture of ACN:TEA:H_2O (v:v:v)) was confirmed via FT-IR studies, as shown for exemplary spectra - and the corresponding differential spectra - in Figure S9 indicating no notable spectral changes within the observation period of 1 h. The collected IR data confirms that APS remains stable within the period of active repair (i.e., approx. 30 min) at catalytic conditions. In order to confirm the IR data, ^{1}H NMR spectroscopy was performed clearly indicating that no peak change of the TEA signals was apparent when adding APS to the TEA containing deuterated solvent mixture acetonitrile-d_3/D_2O (8:2, v:v), as shown in the ^{1}H NMR spectra in Figure S6. In contrast, if in the same mixture a ruthenium(II) photosensitizer and oxygen were present, upon irradiation with 470 nm signals associated with TEA decreased with time indicating the reaction of singlet oxygen with TEA (see Figure S7). It its thus rationalized that the $^1O_2$-based repair strategy cannot be applied without solvent exchange. Further evidence for the stability of APS in the solvent mixture used for catalysis (6:3:1, ACN:TEA:H_2O (v:v:v)) comes from UV/Vis spectroscopic investigations, as very little effect on the waiting time between mixing APS with the 6:3:1 solvent mixture and its application for the repair of hydrogenated **$RuPtI_2$** was observed (see Figure S12). Finally, repair of inactive **$RuPtI_2$** with APS also worked out in absence of TEA, excluding the possibility of an APS oxidized TEA species as truly active repair agent (see Figure S13).

Conclusion

In summary, an innovative, simple and very efficient new repair methodology using ammonium persulfate for revitalizing the hydrogen evolution catalyst **$RuPtI_2$** after deactivation was developed. This procedure only requires the *in situ* addition of a solid repair agent, which potentially greatly enhances the utility of the catalyst repair concept for a wide variety of molecular bridging architectures and reductive catalytic reactions. Most notably, the repaired **$RuPtI_2$** catalyst shows an improved catalytic performance vs. the initial catalytic mixture indicating that persulfate is indeed aiding in the primary activation of the catalyst.

This study was facilitated by the non-invasive and *in situ* optical hydrogen detection using advanced rotational Raman spectroscopy with a thermally stabilized vial sample holder that effectively avoids condensation of the solvent and leakage of gaseous reaction products yielding yet unprecedently precise hydrogen concentration data in a continuous fashion. Additionally, this configuration enables a significantly improved reproducibility between individual runs while simultaneously providing higher quality results. Furthermore, only very small sample amounts are required to elucidate catalytic kinetics. The Raman spectroscopic system was for the first time applied during extended observation periods relevant to photocatalysis research with excellent reliability during 700+ hours of continuous operation. Consequently, precise quantitative insight on the kinetics of hydrogen evolution catalysis is provided even during periods of low hydrogen evolution activity. The excellent data quality provided by the NGA enabled the identification of an induction phase, which remained previously undetected given reproducibility limits of GC-based analysis. This is of particular importance for understanding the full catalytic cycle including catalyst activation, deactivation, and repair. Thereby, a previously not detectable induction phase for the pristine **$RuPtI_2$** photocatalytic process was identified.

Future studies with the NGA will focus on the detection of other and/or additional gases relevant in artificial photosynthesis, to demonstrate the versatility of rotational Raman spectroscopy in such complex photocatalytic scenarios. With assets such as short measurement times, automated sampling, *in situ* non-destructive analysis and in the future potentially fiber optically coupled multiplexing, the optimization of reaction parameters, repair mechanisms and the effects of different illumination schemes may be studied in a highly parallelized fashion, accelerating the discovery of optimized photocatalyst/repair systems for efficient artificial photosynthesis.

Experimental Section

Comprehensive experimental procedures were placed in the Supporting Information.

Acknowledgements

The members of the Institute of Analytical and Bioanalytical Chemistry (IABC) at Ulm University are thanked for support and scientific discussion. Special thanks also to Jesper Schwarz for scientific exchange. B.B. acknowledges support by the Studienstiftung des Deutschen Volkes for a PhD fellowship. All authors acknowledge the Deutsche Forschungsgesellschaft (DFG, German Science Foundation) for funding within the Sonderforschungsbereich (SFB) TRR 234 CataLight (project number 364549901; project C2 and A1). Open Access funding enabled and organized by Projekt DEAL.

Conflict of Interest

The authors declare no conflict of interest.

Data Availability Statement

The data that support the findings of this study are available from the corresponding author upon reasonable request.

Keywords: Active Repair · Gas Analysis · Photocatalytic Hydrogen Production · Raman Spectroscopy

[1] C. Acar, I. Dincer, C. Zamfirescu, *Int. J. Energy Res.* **2014**, *38*, 1903–1920.
[2] K. Kalyanasundaram, *Coord. Chem. Rev.* **1982**, *46*, 159–244.
[3] N. S. Lewis, D. G. Nocera, *Proc. Natl. Acad. Sci. USA* **2006**, *103*, 15729–15735.
[4] E. S. Andreiadis, M. Chavarot-Kerlidou, M. Fontecave, V. Artero, *Photochem. Photobiol.* **2011**, *87*, 946–964.
[5] W. Lubitz, W. Tumas, *Chem. Rev.* **2007**, *107*, 3900–3903.
[6] Y. Huang, D. Li, S. Feng, Y. Jia, S. Guo, X. Wu, M. Chen, W. Shi, *Angew. Chem. Int. Ed.* **2022**, *61*, e200212234.
[7] D. Gust, D. Kramer, A. Moore, T. A. Moore, W. Vermaas, *MRS Bull.* **2008**, *33*, 383–387.
[8] L. Hammarström, *Curr. Opin. Chem. Biol.* **2003**, *7*, 666–673.
[9] J. Barber, *Chem. Soc. Rev.* **2009**, *38*, 185–196.
[10] A. C. Benniston, A. Harriman, *Mater. Today* **2008**, *11*, 26–34.
[11] F. Scalambra, I. F. Díaz-Ortega, A. Romerosa, *Dalton Trans.* **2022**, *51*, 14022–14031.
[12] M. Lämmle, A. K. Mengele, G. E. Shillito, S. Kupfer, S. Rau, *Chem. Eur. J.* **2023**, *29*, e202202722.
[13] S. Yang, D. Fan, W. Hu, B. Pattengale, C. Liu, X. Zhang, J. Huang, *J. Phys. Chem. C* **2018**, *122*, 3305–3311.
[14] D. Kim, D. R. Whang, S. Y. Park, *J. Am. Chem. Soc.* **2016**, *138*, 8698–8701.
[15] A. E. Thorarinsdottir, S. S. Veroneau, D. G. Nocera, *Nat. Commun.* **2022**, *13*, 1243.
[16] A. K. Mengele, S. Rau, *JACS Au* **2023**, *3*, 36–46.
[17] M. G. Pfeffer, T. Kowacs, M. Wächtler, J. Guthmuller, B. Dietzek, J. G. Vos, S. Rau, *Angew. Chem. Int. Ed.* **2015**, *54*, 6627–6631.
[18] M. G. Pfeffer, C. Müller, E. T. E. Kastl, A. K. Mengele, B. Bagemihl, S. S. Fauth, J. Habermehl, L. Petermann, M. Wächtler, M. Schulz, D. Chartrand, F. Laverdière, P. Seeber, S. Kupfer, S. Gräfe, G. S. Hanan, J. G. Vos, B. Dietzek-ivanšić, S. Rau, *Nat. Chem.* **2022**, *14*, 500–506.
[19] D. R. Whang, S. Y. Park, *ChemSusChem* **2015**, *8*, 3204–3207.
[20] D. Mislov, M. Cifrek, I. Krois, H. Dzapo, *2015 IEEE Sensors Appl. Symp.* **2015**, 1–5.
[21] J. Park, J. H. Chang, M. Choi, J. J. Pak, D. Y. Lee, Y. K. Pak, *Sensors 2007 IEEE* **2007**, 1412–1415.
[22] L. Li, L. Duan, F. Wen, C. Li, M. Wang, A. Hagfeldt, L. Sun, *Chem. Commun.* **2012**, *48*, 988–990.
[23] R. Wang, F. P. Healey, J. Myers, *Plant Physiol.* **1971**, *48*, 108–110.
[24] S. F. Silva, L. Coelho, O. Frazão, J. L. Santos, F. X. Malcata, *IEEE Sens. J.* **2012**, *12*, 93–102.
[25] R. T. Wang, *Methods Enzymol.* **1980**, *69*, 409–413.
[26] J. Kund, J. Romer, E. Oswald, A. Gaus, M. Küllmer, A. Turchanin, M. Delius, C. Kranz, *ChemElectroChem* **2022**, *9*, e202200071.
[27] E. Oswald, A. L. Gaus, J. Kund, M. Küllmer, J. Romer, S. Weizenegger, T. Ullrich, A. K. Mengele, L. Petermann, R. Leiter, P. R. Unwin, U. Kaiser, S. Rau, A. Kahnt, A. Turchanin, M. von Delius, C. Kranz, *Chem. Eur. J.* **2021**, *27*, 16896–16903.
[28] J. Lee, H. Ye, S. Pan, A. J. Bard, *Anal. Chem.* **2008**, *80*, 7445–7450.
[29] D. Shevela, J. Messinger, *Front. Plant Sci.* **2013**, *4*, 473.
[30] C. Castro-Castillo, F. Armijo, M. Isaacs, E. Pastor, G. García, *Electrochem. Commun.* **2020**, *118*, 106809.
[31] D. K. Dogutan, D. G. Nocera, *Acc. Chem. Res.* **2019**, *52*, 3143–3148.
[32] B. D. MacCraith, C. M. McDonagh, G. O'Keeffe, E. T. Keyes, J. G. Vos, B. O'Kelly, J. F. McGilp, *Analyst* **1993**, *118*, 385–388.
[33] X. Lu, M. A. Winnik, *Chem. Mater.* **2001**, *13*, 3449–3463.
[34] O. S. Wolfbeis, *BioEssays* **2015**, *37*, 921–928.
[35] F. L. Huber, S. Amthor, B. Schwarz, B. Mizaikoff, C. Streb, S. Rau, *Sustain. Energy Fuels* **2018**, *2*, 1974–1978.
[36] M. Sender, F. L. Huber, M. C. G. Moersch, D. Kowalczyk, J. Hniopek, S. Klingler, M. Schmitt, S. Kaufhold, K. Siewerth, J. Popp, B. Mizaikoff, D. Ziegenbalg, S. Rau, *ChemSusChem* **2022**, *15*, e202200708.
[37] S. Klingler, J. Hniopek, R. Stach, M. Schmitt, J. Popp, B. Mizaikoff, *ACS Meas. Sci. Au* **2022**, *2*, 157–166.
[38] D. Schiel, W. Richter, *Fresenius Z. Anal. Chem.* **1987**, *327*, 335–337.
[39] J. Schwarz, A. Ilic, S. Kaufhold, J. Ahokas, P. Myllyperkiö, M. Pettersson, K. Wärnmark, *Sustain. Energy Fuels* **2022**, *6*, 4388–4392.
[40] "Method and Device for Determining Gas Concentration": J. Ahokas, M. Pettersson, WO2013079806A1, **2013**.
[41] S. Tschierlei, M. Karnahl, M. Presselt, B. Dietzek, J. Guthmuller, L. González, M. Schmitt, S. Rau, J. Popp, *Angew. Chem. Int. Ed.* **2010**, *49*, 3981–3984.
[42] R. Hara, M. Ishigaki, Y. Ozaki, T. Ahamed, R. Noguchi, A. Miyamoto, T. Genkawa, *Food Chem.* **2021**, *360*, 129896.
[43] H. Ozawa, K. Sakai, *Chem. Commun.* **2011**, *47*, 2227–2242.
[44] P. Lei, M. Hedlund, R. Lomoth, H. Rensmo, O. Johansson, L. Hammarstro, **2008**, 130, 26–27.
[45] M. G. Pfeffer, B. Schäfer, G. Smolentsev, J. Uhlig, E. Nazarenko, J. Guthmuller, C. Kuhnt, M. Wächtler, B. Dietzek, V. Sundström, S. Rau, *Angew. Chem. Int. Ed.* **2015**, *54*, 5044–5048.
[46] K. Khosravi, M. E. Hoque, B. Dimock, H. Hintelmann, C. D. Metcalfe, *Anal. Chim. Acta* **2012**, *713*, 86–91.
[47] S. Wacławek, H. V. Lutze, K. Grübel, V. V. T. Padil, M. Černík, D. D. Dionysiou, *Chem. Eng. J.* **2017**, *330*, 44–62.
[48] K. J. Haunreiter, A. B. Dichiara, R. Gustafson, *ACS Sustainable Chem. Eng.* **2022**, *10*, 3882–3891.
[49] S. Hosseini, J. N. Janusz, M. Tanwar, A. D. Pendergast, M. Neurock, H. S. White, *J. Am. Chem. Soc.* **2022**, *144*, 21103–21115.
[50] C. Kranz, M. Wächtler, *Chem. Soc. Rev.* **2021**, *50*, 1407–1437.
[51] C. Turro, *Nat. Chem.* **2022**, *14*, 487–488.
[52] D. N. Bailey, D. M. Hercules, D. K. Roe, *J. Electrochem. Soc.* **1969**, *116*, 190.
[53] N. U. Day, M. G. Walter, C. C. Wamser, *J. Phys. Chem. C* **2015**, *119*, 17378–17388.
[54] J. Van Kranendonk, G. Karl, *Rev. Mod. Phys.* **1968**, *40*, 531–555.

Manuscript received: May 5, 2023
Accepted manuscript online: July 31, 2023
Version of record online: August 17, 2023